I R A M P
2(1), June 2011, pp. 1-23

ISSN: 2229-3159

REVIEW ARTICLE

Controlling Electron Collisions-Recollisions with Ultrashort Intense Laser Pulses – From Femto to Attosecond Science

ANDRE D BANDRAUK*, SZCZEPAN CHELKOWSKI AND KAI JUN YUAN

Computational Chemistry and Molecular Photonics Laboratory, Université de Sherbrooke, Québec, J1K 2R1, Canada

ABSTRACT: Interaction of intense ultrashort (few-cycle) laser pulses with atoms and molecules leads to a highly nonlinear nonperturbative regime of electron dynamics and response. Ionized electrons are shown to be controlled by such pulses and the response is described by simple classical models of under and above barrier ionization followed by recollision with the parent ion or collision with neighboring ions in molecules. Harmonic generation in such a nonperturbative regime produces photons with maximum energy predicted by simple classical models of collision-recollision for both linearly and circularly polarized pulses. This highly nonlinear generation of high energy photons is currently the main source of attosecond pulses.

1. INTRODUCTION

Advances in current laser technology is providing new tools for experimentalists and challenges for theorists to explore a new regime of light-matter interaction, the nonlinear nonperturbative interaction of atoms and molecules with intense ($I \geq 10^{+14}$ W/cm^2) few cycle laser pulses. Much of the earlier experimental and theoretical work in this new nonperturbative regime of radiation-atom interaction has been summarized by Brabec, Krausz [1], Corkum, Krausz [2]. Thus in the atomic case new nonperturbative optical phenomena have been found such as above threshold ionization, ATI, [1], tunnelling ionization predicted as early as 1980 [3-5] and is the basis of re-collision physics [6] which has been confirmed experimentally recently [7]. Another important nonlinear process, High-Order Harmonic Generation, HHG, is the current most convenient source of attosecond (1asec = 10^{-18}s) pulses [8]. This rapid development of ultrashort intense laser pulses allows nowadays for shaping and focussing such pulses to higher intensities creating electric fields E greater than the atomic unit, a.u, $E_0 = 5\times10^9$ V cm^{-1} at the 1s orbit radius $a_0 = 0.0529$ nm of the H atom. This corresponds to an a.u. of intensity $I_0 = cE_0^2/8\pi = 3.54 \times 10^{16}$ W/cm^2. Such pulses can be compressed to times of several femtoseconds (1 fs= 10^{-15}s), thus creating radiative coherences that are shorter than molecular nonradiative (radiationless) relaxation times [9,10]. We give in table 1 a brief "history" of this evolution (revolution) and the new terminology associated with this evolution. In table 1 we also summarize the atomic units, a.u., for various physical quantities and/or parameters used to describe the physical processes occurring under the "extreme" conditions of these new pulses.

Whereas at the end of the 20th century the focus was on femtosecond (fs) photochemistry and photophysics culminating with a Nobel prize to A. H. Zewail (Caltech) for "Femto Chemistry" [12] a major effort is now underway to develop single attosecond (asec) optical pulses based on the nonperturbative physics of HHG in atoms [8] and MHOHG, Molecular High Order Harmonic Generation in molecules [13]. These new asec pulses presage the control of electron motion in molecules, the "Holy Grail" of many atomic and molecular sciences [14-16].

Canada Research Chair: http://pages.usherbrooke.ca/adbandrauk

Table 1
Evolution of Laser Parameters

Times		*Intensity (Watts/cm²)*		*Year*
Nano	10^{-9}	Giga	10^{+9}	1980
Pico	10^{-12}	Tera	10^{+12}	1990
Femto	10^{-15}	Peta	10^{+15}	1995
1 a.u.: $t_0=24.2\times10^{-18}$		$I_o=3.54\times10^{+16}$		
Atto	10^{-18}	Exa	10^{+18}	2001
Zepto	10^{-21}	Zetta	10^{+21}	2009
Yocto	10^{-24}	Yotta	10^{+24}	?

The Schwinger limit, 10^{+29} W/cm^2, is the limit of instability of matter by tunneling from the vacuum itself thus creating electron-positron pairs [11].

Table 2
Atomic units ($e = \hbar = m_e = 1$; $c = 137.036$)

Potential energy :	$V_0 = e^2/a_0 = 1$ Hartree $= 27.2$ eV
Electric field :	$E_0 = e/a_0^2 = 5.14 \times 10^9$ V cm^{-1}
Intensity :	$I_0 = cE_0^2/8\pi = 3.54 \times 10^{16}$ W/cm^2
Distance :	$a_0 = 0.0529$ nm
Velocity :	$\upsilon_0 = 2.19 \times 10^8$ cm s^{-1}
Time :	$t_0 = a_0/\upsilon_o = 24.2 \times 10^{-18}$s
	$t_c = \hbar/m_e c^2 = 1.29 \times 10^{-21}$s

The intensities discussed in the present article, $10^{14} \leq I \leq 10^{15}$ W/cm^2 correspond to fields approaching the internal Coulomb potentials V_0 (table 2) in atoms and molecules, thus introducing considerable distortions of intermolecular potentials. Using a dressed photon state representation, such strong radiatively induced distortions create LIMP'S, Laser Induced Molecular Potentials, leading to "bond-softening" via laser-induced avoided crossings of molecular potentials [17, 18]. At these high intensities, one needs to consider further ionization and Above-Threshold Dissociation, ATD, the equivalence of ATI in atoms. Furthermore the quasistatic picture of atomic tunnelling ionization [3-6] needs to be modified in view of the multi-centre nature of electron potentials in molecules and the presence of large radiative transition moments, originally described by Mulliken [19] as Charge Resonance (CR) transitions [17, 18]. One of the fundamental differences between intense field ionization of atoms and molecules is "Enhanced Ionization" which occurs at critical internuclear distances R_c greater than equilibrium distances R_e for molecules exposed to intense pulses [17,18]. Quasistatic models of enhanced ionization have been successful in predicting values of R_c [20-23]. The main tenet of this model, which differs fundamentally from quasistatic atomic ionization is that laser induced charge resonance (CR) effects localize temporarily the electron by charge transfer due to the presence of large electronic transition moments in molecules resulting in adiabatic electronic charge transfer across the whole length of a molecule [19].

The low frequency nonlinear nonperturbative regime of laser-matter interaction is characterized by highly nonlinear multiphoton processes best described by quasistatic semiclassical models of simple tunnelling ionization processes followed by Laser Induced Electron Re-collision, LIERC of the ionized electron with the parent ion [4,6]. It has been applied successfully to explain ATI and HHG in atoms [1], thus offering a nonlinear nonperturbative theoretical framework based on quasistatic models. Molecules offer the possibility of the recolliding electron to "diffract" from more than one nuclear center, leading to a phenomenon, laser-induced electron diffraction, LIED [24], a tool for probing molecular geometry changes on ultrashort time scales. Coulomb explosion, ATI and MHOHG provide other methods using re-collision to image molecules [25] even at the orbital level by "orbital tomography" [26]. Thus laser induced electron re-collision LIERC, is a central process in intense field physics [6]. In atoms it has

led to an efficient source of X-rays and extreme ultraviolet (UV) radiation and to asec optical pulses [2, 8, 16]. In diatomic molecules it is allowing for asec time resolved electron – nuclear dynamics [27-29]. Less well appreciated is the possibility of an electron colliding with a neighbouring ion to generate high order harmonics well beyond the maximum energy in atoms of I_p+3.17U_p, where I_p is the ionization potential, U_p = I/4ω² (in a.u.) is the electron ponderomotive energy at laser intensity I and frequency ω [30-32]. Reflection by a laser-driven electron from a neighbouring ion followed by recombination at a parent ion can also lead to harmonics by acquiring electron ponderomotive energies up to 32 U_p [33, 34].

Clearly, atomic and molecular phenomena in ultrashort intense laser fields can be considered as an extension of the principles of coherent control [35, 36] into the nonlinear nonperturbative regime of laser-matter interactions. One of the fundamental concepts of intense field laser-atom interaction has been the rescattering or three-step model [4, 6]. Thus following ionization, the electron remains controlled by the laser pulse, returning to the ion core after a phase and sign change in the electric field of the laser pulse. Molecules exposed to intense laser fields add a new perspective to the study of intense laser-matter interactions. The extra degrees of freedom from nuclear motion allow for "entanglement" of the electron-nuclear dynamics thus complicating the laser control of molecular processes at high intensities. Nevertheless, extension of the simple semi classical atomic re-collision model has led to elucidation of molecular charge-resonance-enhanced ionization, CREI, which occurs in molecules at large internuclear distances. The electron re-collision model has now been validated experimentally in molecules [37] and is becoming a new tool for probing molecular dynamics on ultrashort time scales [24-27]. To date the model has been limited to linear polarised pulses, thus controlling the ionized electron to move in linear trajectories. New research with ionization by ultrashort intense circularly polarized pulses in molecules [38,39] is opening new theoretical questions and generating new models where electron combination and recombination is again the main concept elucidating strong field physics phenomena.

2. QUASISTATIC MODELS: ONE-ELECTRON SYSTEMS IN STRONG FIELDS

The first simple analytic formulae for atomic multiphoton ionization beyond usual perturbation (Fermi Golden rule) theory was obtained by Keldysh [3] who showed that a parameter γ, today called the Keldysh parameter [40, 41] allows to separate the perturbative multiphoton regime from the nonperturbative quasistatic tunnelling regime. This parameter is obtained from the low frequency limit of the transition probability from an initial bound state to a Volkov state, the state of a free electron "dressed" by a laser field [40, 41]. This is essentially a time-dependent Distorted Wave Born Approximation where the Coulomb potential is retained in the initial bound state and the laser field only in the final continuum state. The Keldysh parameter is then defined by [40, 41]

$$\gamma = (I_p / 2U_p)^{1/2} \tag{1}$$

where I_p is the ionization potential and U_p is the ponderomotive energy, U_p = I_0 / 4ω², the average kinetic energy of a free electron in a linearly polarized field $E(t) = E_0 \cos(\omega t)$ and peak intensity $I_0 = cE_0^2/8\pi$ at frequency ω. The ponderomotive energy U_p and ponderomotive radius α_p are in fact two additional important parameters in laser-induced electronic processes. Solving the classical equations of motion in a monochromatic time dependent field $E(t) = E_0 \cos(\omega t + \phi)$ gives in a.u.,

$$\ddot{z} = -E_0 \cos(\omega t + \phi), \dot{z}(t) = -\frac{E_0}{\omega}[\sin(\omega t + \phi) - \sin\phi], \tag{2}$$

$$z(t) = -\frac{E_0}{\omega^2}[\cos\phi - \cos(\omega t + \phi) - \omega_0 t \sin\phi], \tag{3}$$

where φ is the initial laser phase called the CEP (Carrier Envelope Phase) at which moment an electron is ionized at time t = 0 assuming an initial zero velocity $\dot{z}(0) = 0$ as in the tunnelling model [4], from which one can estimate initial ionization rates using a static E field rate [3, 4, 40]. Tunnelling ionization has now been detected in atoms

from the modulation of the ionized electron density by the intense laser field [7]. These classical equations define the ponderomotive radius α_p and ponderomotive energy U_p (in a.u.)

$$\alpha_p = E_0/\omega^2, U_p = \frac{1}{4}\alpha_p\omega^2 = E_0^2/4\omega^2 . \quad (4)$$

The Keldysh parameter γ, equation (1) is a ratio of two energies: I_p the minimum energy to ionize the electron and $2Up$, the maximum kinetic energy, $\frac{1}{2}\dot{z}^2$, acquired by a free electron in the laser field. This simple classical quasistatic model described by equations (2-4) where one assumes an electron is ionized with initial zero velocity $\dot{z}(0) = 0$, the basis of tunnelling ionization models [1, 4] allows us to deduce the laser induced dynamics of the electron after ionization. Thus for λ = 1064 nm (ω = 0.043 a.u.) and intensity $I_0 = 1\times10^{14}$ W/cm^2 = 3×10^{-3}a.u., one obtains α_p = 29 a.u.=1.53nm. This maximum displacement α_p determines the minimum size of numerical grids and U_p determines the corresponding spatio-temporal steps Δx, Δt (from uncertainty principle relations) in computations at high intensities [42]. Equation (2) also allows to predict the maximum average kinetic energy to be $\frac{1}{2}\langle\dot{z}(t)\rangle^2 = 3U_p$ at CEP phase $\phi = \pi/2$ ($\langle\cos^2\omega t\rangle = 1/2$, $\langle\cos\omega t\rangle = 0$). Such high energies acquired during ionization was observed and explained in microwave ATI using the simple model of equations (2-3) [43]. In practice ionization occurs at different phases $\phi = \omega t_0$, i.e, i.e., at time t_0, the instant the electron is created in the field. As we show later, t_0, determines the electron trajectories for collision with neighbouring ions and recollision with the parent ion in both linear and circularly polarized laser fields. Initial zero velocity, $\dot{z}(t_0) = 0$ will occur at the instant of tunnel ionization [4,6].

The quasistatic model allows further for establishing the critical or minimum field E_m where above-barrier ionization occurs instead of under-barrier tunnelling ionization. This is illustrated in Fig. 1(a) for a one-electron atom and Fig. 1(b) for a single valence electron in a diatomic molecule such as H_2^+, in the presence of a static electric field *E*. In the atomic case, where a single "active" electron is bound by an effective nuclear charge q+, the total potential along the field polarization, i.e., *z*-axis , can be written as $V(z) = -q/|z| - Ez$. As seen from Fig. 1(a), the electric field distorts the atomic Coulomb potential thus producing a barrier with a maximum at $z_m = (q/E)^{1/2}$ obtained from $\partial V/\partial z = 0$. Setting $V(z_m) = -I_p$, where I_p is the ionization potential, one obtains the minimum field $E_m = I_p^2/4q$ for above-barrier ionization. For hydrogenic levels, $I_p = -\varepsilon_n = q^2/2n^2$, for a level of principal quantum number *n*. For such a level, the minimum electric field E_m for atomic above-barrier ionization is $E_m = q^4/(2n)^4$ a.u. or intensity $I_m = q^6/(2n)^8$ a.u. Thus for the n = 1 (1s) level of H, I_p = 1/2, I_m =1.4×10^{14} W/cm^2. For the Th^{+89} ion in its $n = 2$ level, $I_m = 90^6/2^{16}$a.u.= 2.84×10^{23}W/cm^2. Such superintense fields are being currently considered in the European ELI (Extreme Light Infrastructure) project [44]. The theoretical description of superintense field electron ionization requires applying the relativistic Dirac equation to such processes and is becoming a new active field of research [45-47].

Molecular above-barrier ionization leads to a new concept, CREI (Charge Resonance Enhanced Ionization) for which recent experiments are summarized in [20]. As illustrated in Fig. 1(b), a molecular electronic potential is a multicenter potential. Atomic energy levels are transformed into delocalized molecular orbitals, MO's, which at large internuclear distance R become linear combinations of atomic orbitals. In the case of H_2^+, the two most important MO's in low frequency multiphoton processes are the HOMO, highest occupied MO and LUMO, lowest unoccupied MO, as these couple radiatively through an electronic transition moment <HOMU|*z*|LUMO>=*R*/2 [18,19]. In the presence of a static field, the LUMO is Stark-shifted in energy by +*ER*/2 whereas the HOMO's energy is lowered by –*ER*/2. Thus, at some critical internuclear distance R_c and critical field E_m, the LUMO, which is populated by the field, ionizes by ionization over the barrier between the two nuclei. This simple quasistatic model was first proposed by Codling *et al.* [48,49] neglecting the Stark energies of both HOMO and LUMO, but rather emphasizing

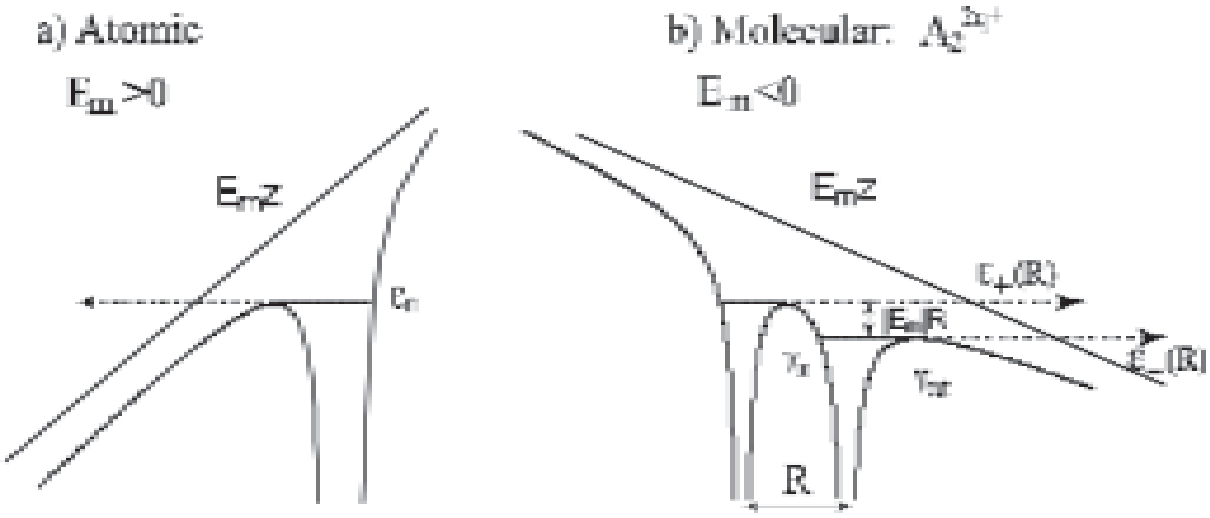

Figure 1: Above Barrier Ionization in (a) Atoms and (b) Molecules

the localization (suppression of the tunnelling) between the field free wells, Fig. 1. Inclusion of the Stark energy shift of the LUMO allows for estimates of R_c and E_m for above-barrier ionization in symmetric diatomic molecules [22, 50]. Inclusion of static dipole moments such as in HeH^{++} further generalizes the concept of CREI in nonsymmetric molecules [51].

We follow the original 1-D model of one-electron molecular ionization in A_2^{2q+} systems where $q+$ is the charge on each nucleus [22, 50]. Exact Born-Oppenheimer (static nuclei) time-dependent Schrödinger, TDSE simulations of highly charged diatomic molecular ions exhibit ionization maxima for internuclear distances $6 \le R \le 10$ a.u. at "critical" distances R_c for laser polarization parallel to the internuclear axis. Ionization from MO's with densities perpendicular to the intermolecular axis also induces abrupt increase of ionization into atomic plateaus at $R_c \sim 6$ a.u. [51]. The necessary conditions for CREI to occur at R_c is that the upper Stark shifted electronic eigenstate energy $\varepsilon_+(R)$ exceeds the two potential barriers in Fig. 1(b), i.e.

$$V_{out}(R_c) \le V_{in}(R_c) \le \varepsilon_+(R_c), \tag{5}$$

where V_{in} and V_{out} are the inner and outer barriers of field modified the two-center Coulomb potential at the critical field strength E_m,

$$V(z,R) = \frac{-q}{|\frac{R}{2}+z|} - \frac{q}{|\frac{R}{2}-z|} + E_m z, \tag{6}$$

and

$$\varepsilon_+(R) = -qI_p - q/R + E_m R/2. \tag{7}$$

$E_m R/2$ is the energy Stark shift of the LUMO [Fig. 1(b)], I_p is the ionization potential of the neutral atom. Ionization potentials of electrons from the same shell are assumed to scale as $I(\text{ion}) = qI_p$ for an ion of charge q-1. The potential (7) has maxima at z_{in} and z_{out} for $E_m < 0$ as in Fig. 1(b) which are given by

$$z_{out} = R/2 + E_q^{-1/2},\ z_{in} = E_q R^3/32, \tag{8}$$

where $E_q = |E_m| / q$.

Solution of the CREI conditions [equation (5)] by setting $\varepsilon_+(R_c) = V_{out}(R_c) = V_{in}(R_c)$ gives [21, 50],

$$R_c = 4.07/I_p\,,\ |E_m| = 0.139 I_p^2\,. \tag{9}$$

Neglecting the Stark-shift of the LUMO gives the value of $R_c = 3/I_p$ and defines the onset of electron localization due to negligible electron tunnelling between the potential double wells in the unperturbed field free molecule [21, 22, 48, 49]. Equation (8) shows the importance of the static field E_m in Stark-shifting the LUMO energy to $\varepsilon_+(R)$ above the field modified barriers illustrated in Fig. 1(b). Nevertheless the end result is the surprising independence of R_c from field strengths E_m and nuclear charge $q+$, thus establishing CREI as a *universal* intense field nonperturbative phenomenon [20, 51-54].

Nonsymmetric molecules such as the one-electron HeH^{++} [51, 55, 56] present a different nonlinear nonperturbative response due to the presence of a permanent dipole moment. This is illustrated in Fig. 2(a), for $E_m > 0$ and Fig. 2(b) for $E_m < 0$. Thus the HOMO is displaced upwards to $\varepsilon_+(R)$ by $|E_m|\,R/2$ for $E_m > 0$ and becomes resonant (degenerate) with the LUMO, $\varepsilon_-(R)$ which is shifted downwards. Thus enhanced ionization can occur by resonance between these two levels. In the case of the opposite field, $E_m < 0$, Fig. 2(b), both HOMO and LUMO can never cross, thus suppressing the resonance and enhanced ionization. Using the similar static Stark-displaced potential model as in the symmetric diatomic case above, one readily obtains the critical distance R_c for enhanced ionization in nonsymmetric systems [53] to occur for $E_m > 0$ at,

$$R_c = \frac{(I_1 - I_2) + [(I_1 - I_2) - 4|E_m|(Z_1 - Z_2)]^{1/2}}{2|E_m|} \tag{10}$$

I_1 and I_2 are the ionization potentials of the different heteroatoms with $I_1 > I_2$ and effective nuclear charges Z_1, Z_2. Numerical TDSE simulations for HeH^{++} where $Z_1 = 2$ and $Z_1 = 1$ show for this nonsymmetric system dependence of R_c on the CEP phase of the field strength E_m and charge separation Z_1-Z_2 as predicted by equation (10) [55].

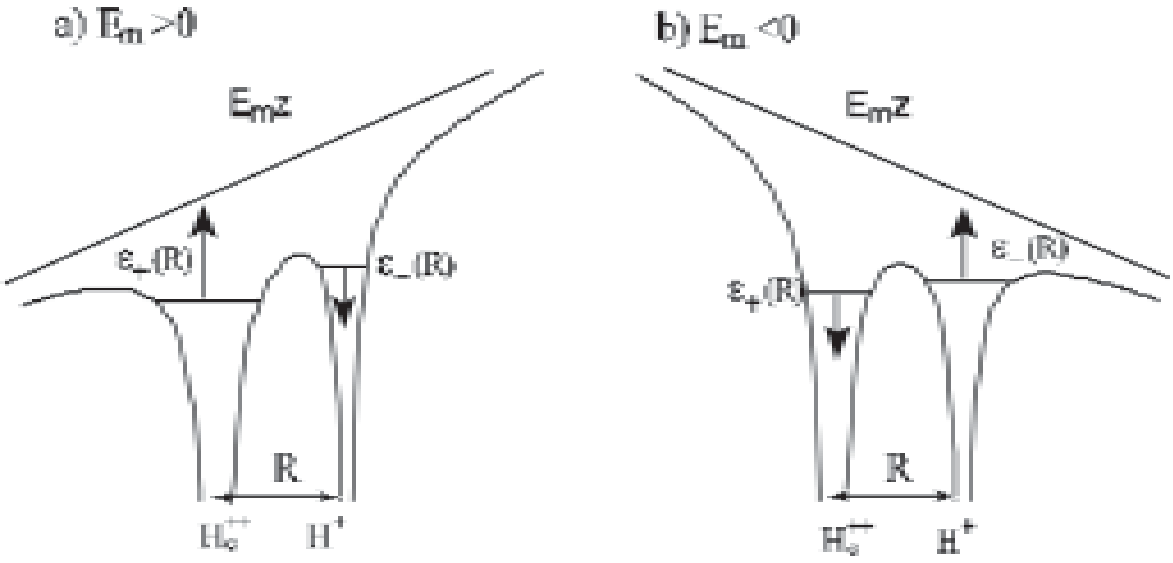

Figure 2: Enhanced Ionization in HeH^{++} by Stark-shifted Orbital ε_+, ε_-

3. LASER INDUCED ELECTRON RECOLLISION – LIERC

In the previous section we have demonstrated that ionization at low frequencies ω and high intensities I can be considered as tunnelling ionization below the Stark induced Coulomb barriers and as above-barrier ionization as illustrated in Figs. 1-2. Subsequent to such ionization, ionized electrons are controlled by the laser field as the Coulomb potentials become less and less relevant. Therefore at high intensities I and low frequencies ω, the freed electron in laser fields can be treated by classical physics, leading thus to early predictions of large electron energies between 2 and 3 U_p in the microwave region [43] and in ATI spectra [5], the latter in agreement with early perturbative

quantum mechanical pictures [57]. Consideration of the phase ϕ of the electric field and its effect on ionized electron motion led to an early model of LIERC of electrons with surfaces plasmas as an efficient mechanism of energy absorption [58]. High Order Harmonic Generation, HHG in atoms showed emission of high energy photons with an energy maximum or cut-off at $E_{max} = I_p + 3.17U_p$ without a corresponding ATI energy cut-off [59, 60]. Classical models of a recolliding electron with the parent ion [4, 60] after tunnelling ionization confirmed this experimental cut-off law [61]. A subsequent quantum-mechanical treatment [62] assuming direct transfer from an initial bound state to laser-dressed electron continuum states reproduced this universal cut-off law. As indicated in the previous sections, electron ionization by low frequency intense fields in molecules leads to the possibility of electron localization on one nucleus with subsequent collision with a neighbouring nucleus [30-34]. Numerical simulations and models show that in the molecular case, cut-offs, i.e., maximum energy in molecular high order harmonic generation, MHOHG exceed considerably the atomic $I_p + 3.17U_p$ energy maximum [13] and that these new high energy cut-offs can be used to measure interatomic distances [63]. In the present section we derive general classical equations of motion of Laser Induced Electron Recollision, LIERC, with parent ions and collision with neighbouring ions thus addressing the role of various mechanisms in the control of MHOHG: re-collision, Coulomb focusing, initial electron velocity and the validity of simple quasistatic models [64]. In particular we will compare ionization and recombination with intense linear and circular polarization laser pulses.

(a) Linear Polarization

The classical equation of motion of an electron in a linearly polarized laser field $E(t)$ at frequency ω, with arbitrary initial velocity υ_0 at initial time t_0 (in a.u.) are:

$$\ddot{z}(t) = -E_0 \cos(\omega t), \dot{z}(t_0) = \upsilon_0, z(t_0) = z_0 \tag{11}$$

Its general solution, at a final time t_f (starting at the initial time t_0), is

$$\dot{z}_f = \upsilon(t_f) = \upsilon_0 + X \sin\phi_0 - X \sin\phi_f, \tag{12}$$

$$z(t_f) = \frac{\upsilon_0 + X \sin\phi_0}{\omega}(\phi_f - \phi_0) + \frac{X}{\omega}[\cos\phi_f - \cos\phi_0] + z_0, \tag{13}$$

where $X = E_0/\omega$, $\phi_0 = \omega t_0$, and $\phi_f = \omega t_f$. X/ω is the displacement (or the amplitude α_p (equation 11) of the electron's oscillatory motion in the electric field), and ϕ_0 and ϕ_f are the laser phases at initial $t = t_0$ and final $t = t_f$, respectively. From equations (11) and (12) the final velocity υ_f reaches its maximal value $\upsilon_f^{max} = \upsilon_0 + 2X$ at the initial phase $\phi_0 = \pi/2$ and at the final phase $\phi_f = (2n + 1)\pi/2$. If the initial velocity $\upsilon_0 = 0$ the maximum attainable electron kinetic energy is $\upsilon_f^2 = 2X^2 = 8U_p$ where $U_p = X^2/4$ (in a.u.) is the ponderomotive energy. This maximum energy is reached only at positions z_f obtained from equation (3):

$$| z(t_f) - z_0 | = \frac{E_0}{\omega^2}(2n-1)\pi, \; n = 1, 2, 3, \cdots, \tag{14}$$

which is always non-zero. The maximum energy $8U_p$ therefore can only be reached at positions different from the electron's departure point z_0, as already derived earlier in [30-32]. It should be noted that the maximum $8U_p$ energy cannot occur when a one-colour laser is used and the electron is ionized via tunnelling since the electric field at the initial phase $\phi_0 = \pi/2$ is zero and the tunnelling probability is zero as well. Such high kinetic energies can show up only in two-colour schemes and in molecules in which the ionization can occur at one nucleus and the ionizing electrons collides with the neighbouring ions [30,32]. Alternatively, a chirped linearly polarized laser pulse in combination with a static field results in maximum energy HHG with $I_p + 42U_p$ [65].

It was shown earlier [4, 64] that, if the electron's initial velocity υ_0 is zero then the maximum energy that the electron can acquire at the return to its departure point z_0 (that is when $z(t_f) = z_0$) is $E_f = \upsilon_f^2/2 = 3.17314\, U_p$. We show below that this result is also valid for the nonzero initial velocity υ_0; that is, we show that allowing a non-zero initial

velocity υ_0 does not lead to a higher return energy of the electron to its departure point $z = z_0$. In other words, the electron return energy is always less than 3.17314 U_p for any non-zero υ_0. This general result is rather surprising since one might believe that a non-zero υ_0 may lead to higher return energies.

We impose next in equation (13) the condition of the electron return to its departure point z_0; that is, we impose $z(t_f) = z_0$. In general, z_0 is very close to the parent ion placed at $z = 0$. In the original derivation of the HOHG cut-off formula, one assumes that $z(t_f) = z_0 = 0$. Thus, using equation (3) one can express υ_0 as a function of ϕ_0 and ϕ_f, or as function of ϕ_0 and $\Delta = \phi_f - \phi_0$, which is the relative phase between the final and initial times t_f and t_0:

$$\frac{\upsilon_0}{X} = \beta_1 \cos\phi_0 + \beta_2 \sin\phi_0 , \tag{15}$$

where

$$\beta_1 = \frac{1-\cos\Delta}{\Delta}, \beta_2 = \frac{\sin\Delta}{\Delta} - 1. \tag{16}$$

Inserting equation (15) into equation (12), we obtain the following expression for the electron's final velocity v_f at the return time t_f to $z = z_0$:

$$\frac{\upsilon_f}{X} = f(\Delta, \phi_0) = \alpha_1 \cos\phi_0 + \alpha_2 \sin\phi_0 , \tag{17}$$

where

$$\alpha_1 = \beta_1 - \sin\Delta, \;\; \alpha_2 = \beta_2 + 1 - \cos\Delta. \tag{18}$$

The extrema of $f(\phi_0, \Delta)$ which lead to the two equations determining the coordinates of these extrema are:

$$\frac{\partial f}{\partial \Delta} = \frac{d\alpha_1}{d\Delta}\cos\phi_0 + \frac{d\alpha_2}{d\Delta}\sin\phi_0 = 0 , \tag{19}$$

$$\frac{\partial f}{\partial \phi_0} = -\alpha_1 \sin\phi_0 + \alpha_2 \cos\phi_0 = 0 . \tag{20}$$

Solving from equation (9) ϕ_0 as a function of the phase difference Δ, one obtains from equation (20) the following equation determining the phase delay Δ value corresponding to the extrema of the velocity $\upsilon_f = Xf(\phi_0, \Delta)$:

$$F(\Delta) = 2 - 2\Delta \sin\Delta + \cos\Delta\,(\Delta^2 - 2) = 0. \tag{21}$$

The function $F(\Delta)$, has zeros at the Δ_k ($k = 1, 2, 3, ...$) reported in table 3. We also give there the corresponding values of ϕ_0 (calculated from equation (20), which yields $\phi_0 = \arctan[\alpha_2(\Delta_k)/\alpha_1(\Delta_k)]$), as well as the values of final velocities υ_f (at the electron return to its departure point $z = z_0$) obtained from equation (17), and the corresponding electron energy $E_f = \upsilon_f^2/2$. The first zero of the function $F(\Delta)$, $k = 1$, corresponds the maximum value of the final velocity $\upsilon_f = 1.259\,590\,5X$, that is to the kinetic energy at the electron return; $\upsilon_f^2 / 2 = 3.173\,37U$p. The subsequent four extrema (shown in table 1) correspond to lower energies. Results for $k = 1, 3, 5$ have been given previously in [66] with $\upsilon_0 = 0$ imposed. This was attributed to the first return, second return and third return of the electron to the departure point z_0. $k = 2$ corresponds to a minimum. Next extremal values of υ_f can be directly estimated from equation (17) by noting that for large phase Δ the final velocity simplifies to

$$\frac{\upsilon_f}{X} = f(\phi_0, \Delta) \approx -\sin(\Delta + \phi_0) = -\sin(\phi_f), \Delta >> 1. \tag{22}$$

Thus for large phase delays $\Delta >> 1$ the final velocity at the electron return to $z = z_0$ is limited by $|\upsilon_f| < X$ and consequently the final kinetic energy at the electron return $E_f = \upsilon_f^2/2$ never exceeds $2U_p$ at large Δ values. Thus we

have proved that the electron final velocity $|\upsilon_f|$ never exceeds $\upsilon_{max} = 1.259\ 590\ 5X$, leading to the maximal energy at the electron return to its departure point $E_f = 3.173\ 137\ U_p$, even when one allows for non-zero initial velocity υ_0. We show next that for all extrema of υ_f shown in table 1 the initial velocity is zero. Firstly, we find from equation (20) that $\tan(\phi_0) = \alpha_1/\alpha_2$. Inserting this result into equation (19) one obtains

$$\frac{\upsilon_0}{X} = \cos\phi_0(\beta_1 + \beta_2 \frac{\alpha_2}{\alpha_1}) = \frac{\cos\phi_0}{\alpha_1 \Delta^2} F(\Delta) . \tag{23}$$

Since υ_0 is now proportional to $F(\Delta)$, therefore we conclude from equation (21) that at any extremum of the function $f(\Delta, \phi_0)$ the initial velocity υ_0 is zero. Clearly the highest energies at the electron return occur when $\upsilon_0 = 0$.

Table 3
Coordinates Δ_k and $\phi_{0,k}$, for k = 1, ···, 5 of the Extrema of the Function $\upsilon_f / X = f(\phi_0, \Delta)$ (equation (17)).

k	*1*	*2*	*3*	*4*	*5*
Δ_k/π	1.3005	2.426 5	3.43 5	4.458	5.461
Δ_0/π	0.0997607	0.0367498	0.032395	0.02079	0.019342 5
ϕ_f/π	1.40024	2.463 2	3.467 4	4.478 8	5.480 34
υ_f/X	1.259 59	0.878 15	1.096 4	0.931 13	1.059 7
E_f/U_p	3.173 14	1.542 3	2.404 3	1.734	2.246

When using UV (or extreme ultraviolet) pulses superposed on femtosecond IR laser pulses, as in attosecond control of MHOHG [67], the electron escapes to the continuum driven by a femtosecond IR laser electric field, with non-zero initial velocity υ_0 due to the absorption of a UV photon. Since harmonics are also generated by the returning electron in theses case, we derive next the corresponding maximal initial velocity, still requiring the electron to return to its departure point. We obtain extrema of the function $\upsilon_0 / X = h(\Delta, \phi_0)$, equation (23) by imposing the conditions as for υ_f / X, equation (17),

$$\frac{\partial h}{\partial \Delta} = \frac{d\beta_1}{d\Delta}\cos\phi_0 + \frac{d\beta_2}{d\Delta}\sin\phi_0 = 0 , \tag{24}$$

$$\frac{\partial h}{\partial \phi_0} = -\beta_1 \sin\phi_0 + \beta_2 \cos\phi_0 = 0 . \tag{25}$$

where β_1 and β_2 are defined in equation (16). These conditions lead again to $F(\Delta) = 0$ as equation (21). The extrema of the function $h(\Delta, \phi_0)$ occur at the same values of $\Delta = \Delta_k$ as in the case of the final velocity υ_f function equation (22), but at different phase ϕ_0 and ϕ_k values, which can be calculated from equation (25):

$$\phi_0 = \arctan\left[\frac{\beta_2(\Delta)}{\beta_1(\Delta)}\right]. \tag{26}$$

We list in table 4 the value of values of ϕ_0, ϕ_0 and υ_0 corresponding to each Δ_k.

For large Δ, equation (15) simplifies to $\upsilon_0 / X \approx \sin(\phi_0)$ which means that $|\upsilon_0 / X| < 1$. This result and table 4 lead us to the conclusion that

$$|\upsilon_0| < \upsilon_{max} = 1.25959X = 1.25959\frac{E_0}{\omega_1} . \tag{27}$$

Table 4
Coordinates Δ_k and $\phi_{0,k}$, for k = 1,...,5 of the Extrema of the Function $\upsilon_0 / X = h(\phi_0, \Delta)$ (equation (23))

k	*1*	*2*	*3*	*4*	*5*
Δ_k / π	1.300 48	2.426 5	3.435	4.458	5.461
ϕ_0 / π	-0.400 24	-0.463 25	-0.467 6	-0.478 8	-0.480 3
ϕ_f / π	0.900 24	1.963 2	2.967 4	3.979 2	4.980 7
υ_0/X	1.259 59	0.878 15	1.096 4	0.931 28	1.059 9

In conclusion, if one initializes the classical trajectory with the initial velocity υ_0 exceeding υ_{max} the electron will never return to its starting point $z = z_0$ (this is true for all possible initial phases ϕ_0) and, consequently, no harmonic generation occurs for high initial velocities $|\upsilon_0|$. υ_{max} coincides with the maximum return velocity found originally by Corkum [2] and derived here from equations (19) and (20). Figure 3 confirms what we have shown analytically, namely that a non-zero υ_0 always lowers the electron energy at its return. In experiments using a 800 nm laser pulse and an asec UV laser pulse, usually a non-zero initial velocity υ_0 will appear for sufficiently high UV frequency [67]. Thus, if one wishes to use an asec pulse to control harmonic generation, one should not introduce initial velocities higher than $0.8 X = 0.8 E_0 / \omega$, since otherwise the electron energy at its return is less than $2.5 U_p$, (see Fig. 3). However, a smaller υ_0 can be useful for the control of harmonic generation without decreasing substantially the cut-off energy, as seen from Fig. 3. ϕ_0 can be controlled via the time delay between fs and asec pulses.

We deduce from Fig. 3 that by varying the initial phase ϕ_0 within an interval $-0.4\,\pi < \phi_0 < 0.4\pi$, and simultaneously maintaining υ_0 within the range $-0.6 X < \upsilon_0 < X$, we will obtain energetic electrons, with $E_f > 2.2 U_p$, within the phase range $1.25\,p < \phi_f < 1.5\,\pi$ whereas, if one uses a single laser pulse, high harmonics are generated, at a fixed value $\phi_f = 1.4\,\pi$. Thus, by varying the delay between an asec and intense IR pulses, we modify the phase at which high harmonic generation (or generation of a new asec pulse) occurs with respect to the phase of an IR pulse. Figure 3 clarifies this new possibility for control; by choosing a specific value of υ_0. Fast electrons return to $z = z_0$ only when initialized within a narrow interval of ϕ_0. For $\upsilon_0 = 0$ this interval is $0.04\,\pi < \phi_0 < 0.18$, whereas for $\upsilon_0 = 0.4 X$ the interval is $-0.09\,\pi < \phi_0 < 0.02\,\pi$, as seen in Fig. 3. Clearly, by allowing for a non-zero initial velocity υ_0 we can create possibilities for MOHG in a much broader interval of initial phases than in standard tunnelling models, in which the initial velocity $\upsilon_0 = 0$ restricts classical trajectories to a very narrow initial ϕ_0 interval.

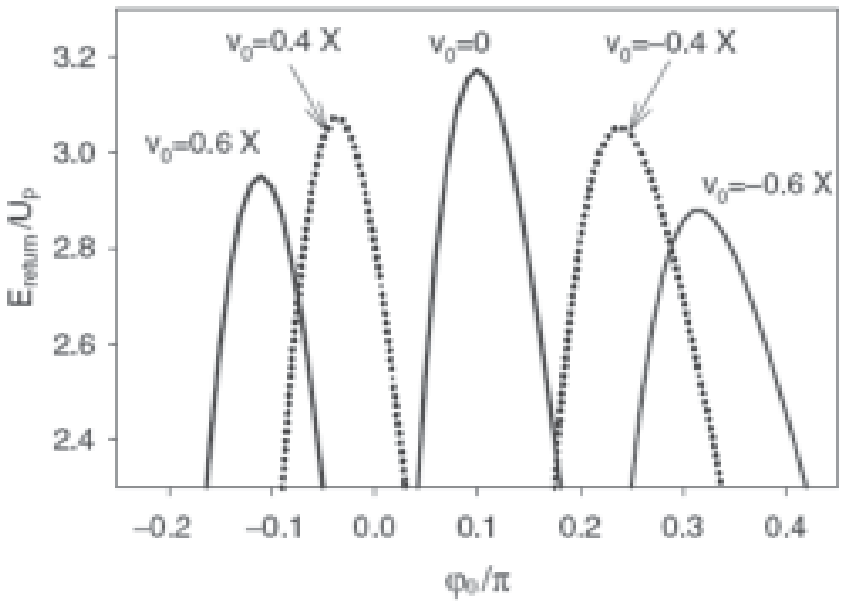

Figure 3: Electron Return Energy (in U_p) as a Function of the Initial Phase ϕ_0 Calculated at Fix υ_0

We now illustrate by quantum computation the effect of recollision dynamics on the HHG spectrum of a single-active electron, SAE, model He with a linearly polarized field $E(t)$ along the z-axis. We add the linearly polarized laser-electron radiative interaction $V_E(r, t) = r \cos\theta\, E(t)$ to the He SAE effective potential [64]:

$$V_c(r) = -\frac{1}{r} - \left(\frac{1}{r} + \frac{k}{2}\right)\exp(-kr) \tag{28}$$

where k = 17/8. The numerical solutions of the TDSE yield an ionization potential I_p of the ground state of this potential to be 24.0 eV as compared to the experimental value 24.6 eV. We use two pulses $E_j(t)$, j=1,2, each defined by vector potentials A_j(t):

$$E_j(t) = -\frac{1}{c}\frac{\partial A_j(t)}{\partial t},\ A_j(t) = -c\varepsilon_j(t)\sin[\omega_j(t-t_j)] \tag{29}$$

with envelope $\varepsilon_j(t)$

$$\varepsilon_j(t) = E_{0,j}\cos^2\left[\frac{\pi(t-t_j)/2}{\tau_j}\right], \tag{30}$$

corresponding to a full width at half-maximum $\Delta t_j = 0.364\tau_j$. The definition of $E_j(t)$ by equations (30-31) ensures the total area $\int_{-\infty}^{\infty} E_j(t)dt = 0$ as required from Maxwell's equations [1].

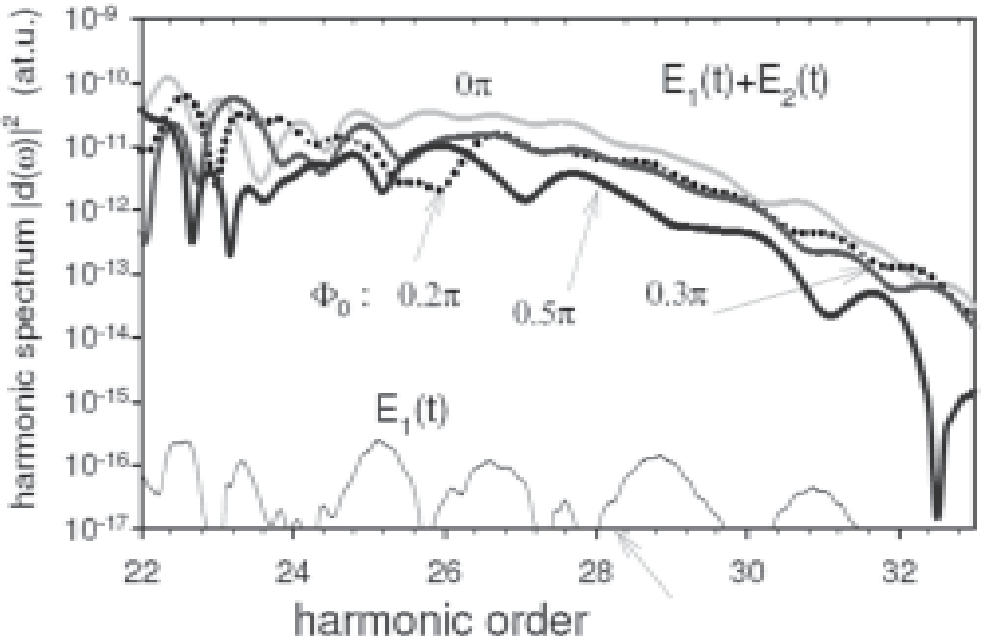

Figure 4: Harmonic Generation Spectrum for a Helium Atom for Various Phase $\Phi_0 = \omega\tau_d$ Delays between asec and IR Pulses. The Intensity of each Pulse is I = 10^{14} W/cm^2 and the Pulse Durations are 10 and 0.6 fs. The Cut off Occurs at $I_p + 3.17U_p = 29\omega$ (ω = 0.057 a.u., λ = 800 nm)

Using Δt_1 =10fs for the IR (λ = 800 nm, ω = 0.057 a.u.), and Δt_2 = 0.6 fs for the asec UV pulse (λ = 115 nm, ω = 0.466 a.u.), the HHG spectrum of the SAE model He was calculated from the FT (Fourier Transform) of the electron acceleration for the linear laser polarization (z-axis)

$$a(t) = \langle \psi(t) | -\partial V / \partial z - E(t) | \psi(t) \rangle,\ a_F(\omega) = \int \exp(-i\omega t) a(t) dt \tag{31}$$

described in [13]. The spectrum is illustrated in Fig. 4 as the square of the dipole spectrum $|d_F(\omega)|^2 = |a_F(\omega)/\omega^2|^2$ for a series of time delays $\tau_d = t_2 - t_1$ with the corresponding phase delays $\phi_0 = \omega_1 \tau_d$ of the IR pulse $E_1(t)$ with respect to the peak of the asec pulse $E_2(t)$. The two-colour laser field, equation (29) corresponds to the combination of each pulse with same intensity $I = 10^{14}$ W/cm^2. Furthermore the spectrum significantly depends on the phase delay ϕ_0 between both pulses. A variation of harmonic intensities by nearly one order of magnitude as a function of ϕ_0 is evident reflecting the different ionization probabilities [68, 69]. Both effects of similar magnitude were already observed in H_2^+ [67], for which the most effective phase delay was $\phi_0 = 0.2\pi$ due to the stronger Coulomb potential. Fig. 4 shows that in the atomic He case the strongest HHG occurs at $\phi_0 = 0$ at the maxima of the IR field $E_1(t)$. At intensity $I = 10^{14}$W/cm^2, $\lambda = 800$nm ($\omega = 0.057$a.u.), $U_p = I / 4\omega^2 = 4.2\omega$ and $I_p = 24.6$eV$=16\omega$, thus defining a cut-off at $I_p + 3.17U_p = 29\omega$, in agreement with Fig. 4 where for harmonic order $N > 30$, the HHG spectrum decreases rapidly. Fig. 4 shows therefore that prior ionization of a bound electron, thus giving it nonzero initial velocity υ_0 generates harmonics with maximum energy at $I_p + 3.17U_p$, the universal cut-off law in HHG from atoms by recollision.

(b) Circularly Polarized Pulses

Atomic HHG by recollision of electrons with circularly polarized pulses is considered impossible since the ionized electron acquires very high angular momentum in the continuum. As the harmonic emission is by a single photon involving a single momentum change from the continuum back to the initial ground state, such a process is highly forbidden. Under special conditions an ionized electron in a circularly polarized field can also collide with inner electrons [39]. In molecular systems, as shown in equation (14), collision of an electron with a neighbouring atom in an intense linearly polarized pulse parallel to the internuclear axis will generate harmonics with maximum energy $8U_p$ at internuclear distances $R = (2n + 1)\pi E_0 / \omega^2$ ($n = 0, 1, ...$) [30-32, 63, 70-72]. The resulting very high energy linearly polarized harmonics in general can be generated in a pre-dissociated molecular gas for asec pulse generation [73]. Atomic circularly polarized HHG by two colour (bichromatic) co-planar circularly polarized counterrotating in the same plane was shown to be possible provided the electron trajectories responsible for the emission have a nonzero initial velocity υ_0. The strongest contribution to the harmonic emission rates comes from those orbits with short travel and return times of 1/3 of a cycle [74] as compared to 2/3 of a cycle for linear polarization [65]. Recent measurements of MHOHG polarization of diatomics in linearly polarized laser fields shows that harmonics are in fact strongly elliptically polarized [75]. Such elliptically polarized MHOHG spectra occur also in extended (large R) H_2^+ simulations with bichromatic ultrashort intense circularly polarized laser pulses [38].

In linearly polarized recollision with parent ions, maximum harmonic energies are given from the initial zero velocity ionization model by $I_p + 3.17\ U_p$ [1, 4], and section 2a, whereas collision with neighboring ions gives harmonic energies up to $I_p + 8U_p$ [30, 31, 63, 64]. For circularly polarized laser pulses of maximum amplitude E_0, corresponding to intensity $I_0 = cE_0^2/8\pi$ and frequency ω and carrier envelope phase (CEP) ϕ,

$$E_x(t) = E_0 \cos(\omega t + \phi), E_y(t) = E_0 \sin(\omega t + \phi)\,, \tag{32}$$

the classical field equations of motion [$\ddot{x}(t) = -E_x(t), \ddot{y}(t) = -E_y(t),$] give the laser induced velocities

$$\dot{x}(t) = -\frac{E_0}{\omega}[\sin(\omega t + \phi) - \sin\phi]\,,\ \dot{y}(t) = -\frac{E_0}{\omega}[\cos\phi - \cos(\omega t + \phi)]\,. \tag{33}$$

For initial velocity conditions $\dot{x}(0) = \dot{y}(0) = 0$ the corresponding displacements are,

$$x(t) = -\frac{E_0}{\omega^2}[\cos\phi - \cos(\omega t + \phi) - \omega t \sin\phi], y(t) = -\frac{E_0}{\omega^2}[\omega t \cos\phi + \sin\phi - \sin(\omega t + \phi)]\,. \tag{34}$$

The total time dependent energy is from equation (33)

$$K_e(t) = \frac{1}{2}[\dot{x}^2(t) + \dot{y}^2(t)] = \left(\frac{E_0}{\omega}\right)^2 (1 - \cos\omega t)\,, \tag{35}$$

with maximum value $8U_p$ at $\omega t_c = (2n+1)\pi$, n = 0, 1, 2, ..., where t_c is collision time, and ponderomotive energy $U_p = E_0^2 / 4\omega^2$. The corresponding maximum electron displacement (transfer) to a neighboring ion is from equation (35)

$$R_n = \sqrt{x^2(t_c) + y^2(t_c)} = \frac{2E_0}{\omega^2}\sqrt{1 + (n + \frac{1}{2})^2\pi^2}\,, \tag{36}$$

for integer n, and is independent of the CEP, ϕ. For diatomic molecules aligned with the x-axis, this reduces to

$$x(t_c) = R_n = -\frac{2E_0}{\omega^2}\left[1 + (n + \frac{1}{2})^2\pi^2\right]\cos\phi, \;\; y(t_c) = 0, \tag{37}$$

where $\tan\phi = -\left(n + \frac{1}{2}\right)\pi$ for collision time t_c.

With a two-color circularly polarized laser field

$$E_x(t) = E_0[\cos(\omega t + \phi_1) + \cos(2\omega t + \phi_2)], E_y(t) = E_0[\sin(\omega t + \phi_1) + \sin(2\omega t + \phi_2)], \tag{38}$$

the CEPs, ϕ_1 and ϕ_2 determine the optimal values of the kinetic energy $K_e(t)$ and electron distance $R(t)$ for MHOHG. The corresponding laser induced velocities are,

$$\dot{x}(t) = -\frac{E_0}{\omega}[\sin(\omega t + \phi_1) - \sin\phi_1 + \cos(\omega t + \phi_2)\sin\omega t], \tag{39a}$$

$$\dot{y}(t) = -\frac{E_0}{\omega}[\cos\phi_1 - \cos(\omega t + \phi_1) + \sin(\omega t + \phi_2)\sin\omega t], \tag{39b}$$

and the corresponding displacements

$$x(t) = -\frac{E_0}{4\omega^2}[4\cos\phi_1 - 4\omega t\sin\phi_1 - 4\cos(\omega t + \phi_1) - \cos(2\omega t + \phi_2) + \cos\phi_2 - 2\omega t\sin\phi_2], \tag{40a}$$

$$y(t) = -\frac{E_0}{4\omega^2}[4\sin\phi_1 + 4\omega t\cos\phi_1 - 4\sin(\omega t + \phi_1) - \sin(2\omega t + \phi_2) + \sin\phi_2 + 2\omega t\cos\phi_2]. \tag{40b}$$

(Maximizing the total kinetic energy $K_e(t)$ with respect to the CEPs ϕ_1 and ϕ_2 gives the net optimal CEP condition $\phi = \phi_1 - \phi_2 = n\pi + \omega t / 2$. Inserting this condition into $K_e(t)$ in equation (35) and maximizing the resulting $K_e(t)$ with respect to $\omega_0 t_c$ gives the result for n = 0, $\omega t_c = 2\pi / 3$, $\phi = \phi_1 - \phi_2 = \pi / 3$ whereas for n = 1, $\omega t_c = 4\pi / 3$, $\phi = -\pi / 3$ [38].

For n = 0, the choice of phases $\omega t_c = 2\pi / 3$, $\phi = \phi_1 - \phi_2 = \pi / 3$ gives respectively the following components of $K_e(t_c)$, where $U_p = E_0^2 / 4\omega^2$,

$$K_{ex}(t_c) = \frac{1}{2}\dot{x}^2(t_c) = \frac{9}{32}\left(\frac{E_0}{\omega}\right)^2 (\sqrt{3}\cos\phi_2 + 3\sin\phi_2)^2, \tag{41a}$$

$$K_{ey}(t_c) = \frac{1}{2}\dot{y}^2(t_c) = \frac{9}{32}\left(\frac{E_0}{\omega}\right)^2 (\sqrt{3}\cos\phi_2 - 3\sin\phi_2)^2, \tag{41b}$$

$$K_e(t_c) = K_{ex}(t_c) + K_{ey}(t_c) = \frac{1}{2}[\dot{x}^2(t_c) + \dot{y}^2(t_c)] = 13.5U_p. \tag{41c}$$

The second choice for $n = 1$, $\omega t_c = 4p/3$, $\phi = -\pi/3$ corresponds to replacing ϕ_2 by $-\phi_1$ in equation (41). Equation (42) shows that the total kinetic energy $K_e(t_c)$ is independent of ϕ_2 for both optimal CEPs $\phi = \pm \pi / 3$.

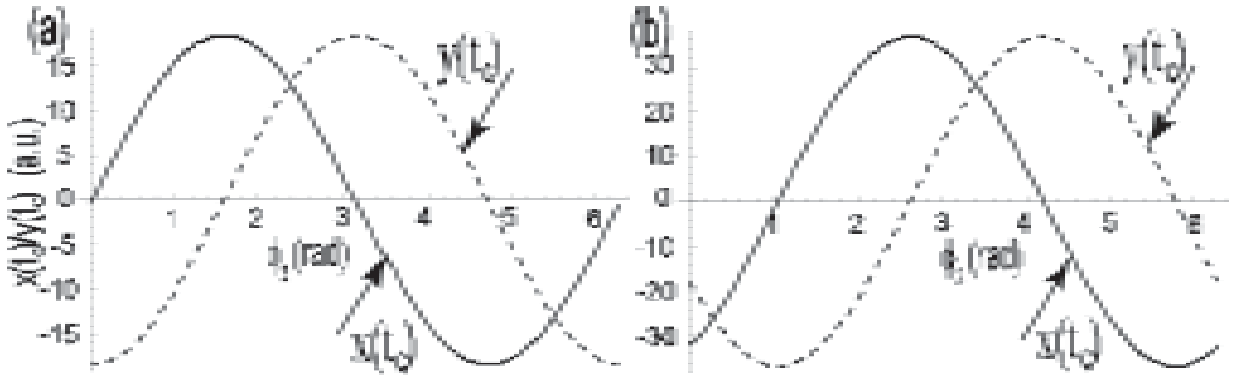

Figure 5: Displacements $x(t_c)$ and $y(t_c)$, Equation (41) for the Cases (a) $n = 0$, $\omega t_c = 2\pi/3$ and (b) $n = 1$, $\omega t_c = 4\pi / 3$ as a Function of ϕ_2. The CEPs $\phi = \phi_1 - \phi_2 = \pi / 3$ and $\phi = -\pi / 3$ give the maximum collision energy $K_e = 13.5U_p$ with a Bichromatic Circularly Polarized Laser Pulse at $I_0 = 2 \times 10^{14}$ Wcm^{-2} ($E_0 = 0.0755$ a.u.), $\lambda_1 = 400$ nm ($\omega = 0.114$ a.u.), and $\lambda_1 = 200$ nm ($2\omega = 0.228$ a.u.)

As examples we consider intensity $I_0 = 2\times10^{14}$ Wcm^{-2} ($E_0 = 0.0755$ a.u.) and $\lambda = 400$nm ($\omega = 0.114$). The electron displacements (transfer distances) $x(t_c)$ and $y(t_c)$ for $\omega t_c = 2\pi/3$, $\phi = \pi/3$ ($n = 0$) and $\omega t_c = 4\pi/3$, $\phi = -\pi/3$ ($n = 1$) are shown in Figs. 5(a) and 5(b), respectively. With $\omega t_c = 2\pi/3$ for example, for phases $\phi_1 = \pi/3$ and $\phi_2 = 0$, the electron displacements are $x(t_c) = -0.35$ a.u. and $y(t_c) = -18.5$ a.u. and for $\phi_1 = 0$ and $\phi_2 = -\pi / 3$, $x(t_c) = -16.2$ a.u. and $y(t_c) = -8.9$ a.u. from equation (40). Maximum efficiency of the MHOHG process is obtained for the *smallest* $x(t_c)$ or $y(t_c)$ which corresponds to near direct (head on) collision with a neighboring nucleus. Thus at $\lambda = 800$nm ($\omega = 0.057$a.u.), the corresponding electron displacements are respectively $x(t_c) = -1.4$ a.u., $y(t_c) = -74$ a.u. and $x(t_c) = -64.6$ a.u., $y(t_c) = -35.7$ a.u.. We conclude hence that short wavelengths (e.g., $\lambda = 400$ nm) and phases $\phi_1 = \pi / 3$, $\phi_2 = 0$ give the best collision conditions with neighboring ions thus increasing MHOHG efficiencies.

As a molecular example we consider the H_2^+ molecular ion at a fixed internuclear separation R (Born-Oppenheimer approximation), interacting with the bichromatic circularly polarized laser pulse $\vec{E}(t)$ equation (39). The corresponding 2D (plane) TDSE is given by

$$i\frac{\partial}{\partial t}\Psi(\vec{r},t) = H(\vec{r},t)\Psi(\vec{r},t), \tag{43}$$

$$H(\vec{r},t) = H_0(\vec{r}) + \vec{r}\cdot\mathrm{E}(t) = -\frac{1}{2}\nabla_{\vec{r}}^2 + V(\vec{r}) + \vec{r}\cdot\vec{\mathrm{E}}(t). \tag{44}$$

$V(\vec{r}) = V(x, y)$ is the two center Coulomb potential and the matter-field interaction is treated in the length gauge. The TDSEs are solved numerically by a three-point difference algorithm combined with higher order split-operator methods [42,76]. A temporal slowly varying envelope $\sin^2(\pi t / 10\tau)$ where $\tau = 2\pi / \omega$ is one optical cycle (o.c.) . The MHOHG power spectra $P_x(\omega)$ and $P_y(\omega)$ are obtained from the absolute square of the Fourier transforms (FT) of the electron acceleration components $a_x(t)$ and $a_y(t)$

$$P_x(\omega) = \left| \int \exp(-i\omega t) a_x(t) dt \right|^2, \quad P_y(\omega) = \left| \int \exp(-i\omega t) a_y(t) dt \right|^2, \tag{45}$$

with the laser induced electron acceleration obtained from the exact time-dependent electron wave function $\Psi(\vec{r}, t)$:

$$a_x(t) = \frac{d^2\langle x \rangle}{dt^2} = -\langle \Psi | \frac{\partial H}{\partial x} | \Psi \rangle, \quad a_y(t) = \frac{d^2\langle y \rangle}{dt^2} = -\langle \Psi | \frac{\partial H}{\partial y} | \Psi \rangle . \tag{46}$$

To describe the polarization properties of the emitted MHOHG, the relevant physical quantities are introduced (see, for example, Fig. 1 in [75]). The power spectra in equation (45) have two *x* and *y* components, thus allowing to extract the dependence of the phase difference δ between the polarized components of the emitted harmonics on the angular frequency ω [78]. The ellipticity ε of MHOHG is defined as

$$\varepsilon = \tan \chi, \tag{47}$$

where

$$\sin(2\chi) = \sin(2\xi) \sin \delta, \quad \tan \xi = \sqrt{P_x / P_y} . \tag{48}$$

In Fig. 6(a), at the intensity $I_0 = 2 \times 10^{14}$ Wcm^{-2} ($E_0 = 0.0755$ a.u.), laser wavelengths λ_1 = 800 nm (ω = 0.057 a.u.), and λ_2 = 400nm (2ω = 0.114 a.u.), and phases $\phi_1 = \pi/3$, and $\phi_2 = 0$ ($\phi = \pi/3$) the maximum harmonic order is obtained: $N_m = (I_p + 13.5U_p)/\omega$ with $y(t_c) = -R = -74$ a.u. and $x(t_c) = -1.4$ a.u. at collision with the neighbor ion. In Fig. 6(b) we show the MHOHG spectrum at the equilibrium distance R_e=2 a.u.. We see the absence of a long plateau with high efficiencies since now collision with neighboring nuclei ***does not*** occur, but rather the H_2^+ molecule at R_e=2 a.u. appears like a one-center atom to the ionized electron at larger *x* and *y*. We reemphasize that at equilibrium as in atoms no collision (recollision) can occur thus resulting in negligible harmonic generation. For longer wavelength in Fig. 6 at 800 nm, a long plateau is obtained with relatively high intensities.

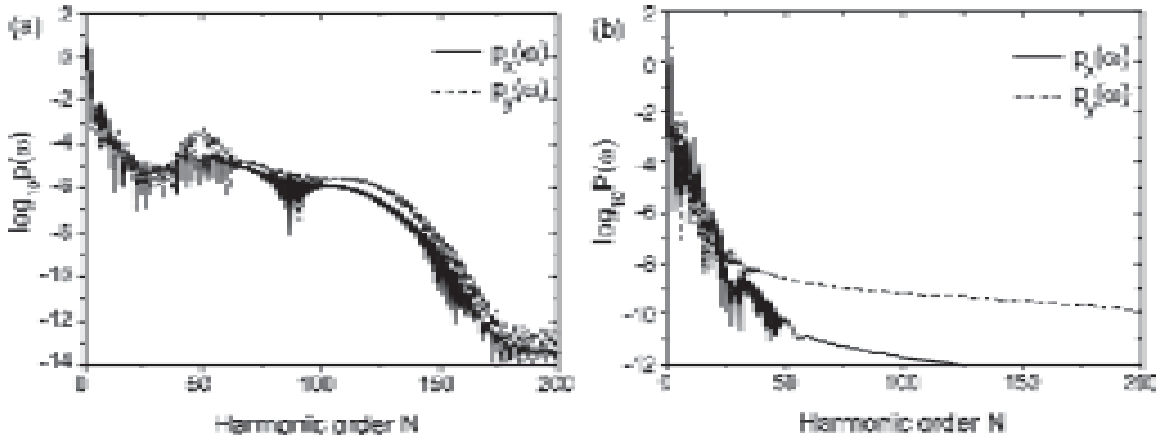

Figure 6: MHOHG Spectra of y-aligned H_2^+ with a Bichromatic Circularly Polarized Laser Pulse at $I_0 = 2 \times 10^{14}$ Wcm^{-2}, λ_1 = 800nm, and λ_2 = 400nm, $\phi_1 = \pi/3$, $\phi_2 = 0$ (a) at $R = -y(t_c) = 74$ a.u. and (b) at $R_e = 2$ a.u.. The cut-off order $N_m = (I_p + 13.5\ \text{Up}) / \omega \approx 120$ for n = 0, $\omega t_c = 2\pi / 3$ and $\phi = \phi_1 - \phi_2 = \pi / 3$

For the polarization properties of the MHOHG emission, in Fig. 7 we show the phase difference δ between the MHOHG *x* and *y* components and absolute values of the ellipticity ε as functions of harmonics order *N* calculated using eqs. (43-46), corresponding to Fig. 6. We note that these polarization properties are very sensitive to the harmonic order *N*, indicating different collision angles of the electron with ions for generation of harmonics. Near the cutoff region where the MHOHG is induced by the electron collision with neighboring ions, the phase δ is π [Fig. 7(a)], producing linearly polarized harmonics emissions with ellipticity | ε | ~ 0 as shown in panels (b), Fig. 7. The emitted MHOHG polarizations can not match the polarization of the driving laser pulses.

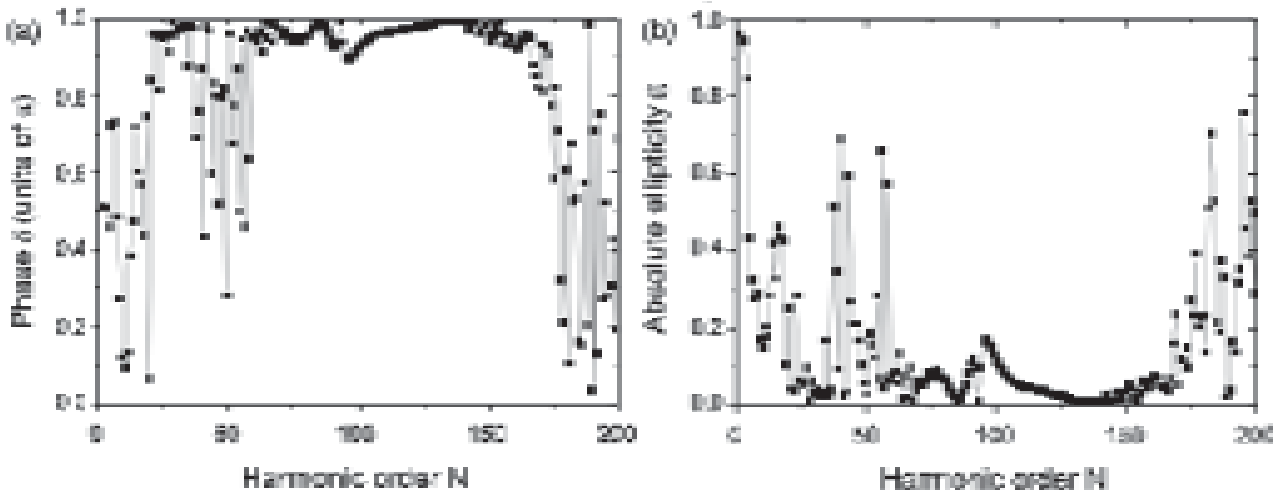

Figure 7: (a): The MHOHG Phase Difference δ between the *x* and *y* Components and (b) Absolute Values of the Ellipticity ε for y-aligned H_2^+ MHOHG at *R* =74 a.u. with a Bichromatic Circularly Polarized Laser Pulse at $I_0 = 2 \times 10^{14}$ Wcm^{-2}, $\lambda_1 = 800$ nm, and $\lambda_2 = 400$ nm, $\phi_1 = \pi/3$, $\phi_2 = 0$, Corresponding to Fig. 6(a)

The present results show that elliptically polarized high order molecular harmonics are generated in a bichromatic ultrashort intense circularly polarized laser pulse for a molecule whose molecular axis is aligned along the laser polarization direction. As reported in [77], the polarization properties are also sensitive to the orientation of molecules in linearly polarized laser fields. Therefore, taking advantage of this effect, the polarization of MHOHG may be enhanced by aligning molecules with proper orientation angle. Moreover, a slightly elliptically polarized driving laser pulses can also be employed for enhancement of the polarization of MHOHG [78]. In conclusion, MHOHG with circularly polarized intense few cycle laser pulses allows for combination by collision of ionized electron with neighboring ions at large internuclear distance *R*. The resulting harmonics are generally elliptically polarized with large maximum energies beyond the atomic recollision cutoff or maximum energy $I_p + 3.17\ U_p$.

4. STRONG FIELD APPROXIMATION AND RECOLLISION

In the previous sections we have presented classical models of collision and recollision of an ionized electron with parent or neighboring ions, resulting in emission of high energy electrons with a cut-off, i.e., a maximum energy limit to $I_p + 3.17U_p$ for recollision with the parent ions and energies beyond depending on the internuclear distance *R* between neighboring ions. A quantum theory of the HHG process has been formulated [62] permitting analytic derivation of the HHG amplitudes under a strong field approximation, SFA, where the influence of the atomic Coulomb potential on the free electron is neglected as compared to the laser field [1-4,79]. As a result the Coulomb continuum eigenfunctions are substituted by field dressed plane waves, called Volkov states [1, 40]. Using the ansatz for the total time dependent electron wave function

$$\Psi(t) = \exp(iI_p t)(|0\rangle + \int d^3\vec{v} b(\vec{v},t)\,|\vec{v}\rangle), \tag{49}$$

where |0> denotes the ground state with ionization potential I_p, and $b(\vec{v}, t)$ is the momentum space amplitude of free electrons, one gets from the TDSE for an atom in the laser electric field $\vec{E}(t)$ [62]

$$b(\vec{v},t) = i\int_{-\infty}^{t} \vec{E}(t')\vec{d}[\vec{p} - \frac{q\vec{A}(t')}{c}]\exp[-iS_1(t',t) + iI_p(t-t')]dt', \tag{50}$$

where $S_1(t',t) = \int_{t'}^{t} dt''\left[\vec{p} - \frac{q}{c}\vec{A}(t'')\right]^2/2$ is called, in [62], the semiclassical action of the electron in the field and q = -|e|=-1 a.u. is the electron charge. The dipole transition moment is defined by $d(\vec{p}) = \langle \vec{p} \,|\, r \,|\, 0\rangle$ which for atomic bound s state is $d \propto p/(p^2 + 2I_p)^3$. The canonical momentum is $\vec{p} = \vec{v} + \frac{q}{c}\vec{A}(t)$ and $A(t)$ is the potential vector defining $\vec{E}(t) = -\frac{1}{c}\frac{\partial \vec{A}}{\partial t}$. From equation (50) one obtains an expression for the laser induced dipole moment at time t [62, 80]

$$\vec{D}(t) = i\int_0^t dt' \int d^3p\ \vec{d}^*(\vec{p} - \frac{q\vec{A}(t)}{c})\vec{E}(t')\cdot\vec{d}(\vec{p} - \frac{q\vec{A}(t')}{c})\exp[-iS_1(t,t') + iI_p(t-t')] + c.c. \tag{51}$$

Equation (51) corresponds to transitions via a resonant continuum state, neglecting contributions from non-resonant states whose contribution vanishes at high laser frequencies (see equation (37) in [81], also [82, 83]). Equation (51) has a simple physical interpretation as a sum of probability amplitudes for field induced various processes [80]: i) $\vec{E}(t')\cdot\vec{d}\left(\vec{p} - \frac{q\vec{A}(t')}{c}\right)$ is the probability amplitude for a bound electron to make transitions to the continuum at time t' with canonical momentum p; (ii) the electron wavefunction is then propagated to time t acquiring a "semiclassical" phase $\exp[-iS_1(t,t')]$, neglecting Coulomb effects as the free electron propagation occurs far from the parent ion; (iii) the electron recombines at time t via the transition moment $\vec{d}^*\left(\vec{p} - \frac{q\vec{A}(t)}{c}\right)$. The factor $I_p(t-t')$ reflects the excess energy the continuum electron has before recombining to the ground state of energy $\varepsilon_n = -I_p$ (Fig. 1).

We now recall a standard definition of the classical action S_c [84] of the electron during its sojourn time in the continuum $\tau = t_f - t_0$ in the field $E(t) = E_0\cos\omega t = -\frac{1}{c}\frac{\partial A}{\partial t}$,

$$S_c = \int_t^{t_f} L(\vec{r},\dot{\vec{r}},t)dt, \qquad L(\vec{r},\dot{\vec{r}},t) = \frac{\dot{\vec{r}}^2}{2} + \frac{q}{c}\dot{\vec{r}}\cdot\vec{A}(t) \tag{52}$$

where $L(\vec{r},\dot{\vec{r}},t)$ is the classical Lagrangian. This definition looks different from the semiclassical action S_1 used in equation (50) and defined in [62]. Our goal now is establish the link between these two definitions of the action. Using the definition of the canonical momentum $\vec{p} = \frac{\partial L}{\partial \dot{\vec{r}}} = \dot{\vec{r}} + \frac{q}{c}\vec{A}(t)$ and the definition of the classical Hamiltonian $H = \vec{p}\cdot\dot{\vec{r}} - L(\vec{r},\dot{\vec{r}},t) = \frac{1}{2}[\vec{p} - \frac{q}{c}\vec{A}(t)]^2$, we obtain the following expression for the standard classical action

$$S_c(t_f,t_0) = \vec{p}\cdot\vec{r}\,|_{t_0}^{t_f} - \int_{t_0}^{t_f}\dot{\vec{p}}\cdot\vec{r}dt - S_1(t_f,t_0), \tag{53}$$

where

$$S_1(t_f,t_0)=\frac{1}{2}\int_{t_0}^{t_f}H(\vec{r},\vec{p},t)dt=\frac{1}{2}\int_{t_0}^{t_f}[\vec{p}-\frac{q}{c}\vec{A}(t)]^2dt\,, \tag{54}$$

is the semiclassical action used in eq. (50) and defined in [62]. The classical equations of motion provide the further relations

$$\dot{\vec{p}}=-\frac{\partial H}{\partial\vec{r}}=0\Rightarrow\vec{p}=\vec{p}(t_0)=\vec{p}(t_f)=\frac{q}{c}\vec{A}(t_0)\,, \tag{55}$$

This gives a new expression for S_c, equation (54):

$$S_c(t_f,t_0)=\vec{p}(t_0)\cdot[\vec{r}(t_f)-\vec{r}(t_0)]-S_1(t_f,t_0)\,. \tag{56}$$

Since for the classical trajectories returning to the tunneling point, we have $\vec{r}(t_f)-\vec{r}(t_0)=0$, therefore we may conclude that for such trajectories both actions differ only by a sign, i.e., $S_c(t_f,t_0)=-S_1(t_f,t_0)$ and they yield the same phase of the electron since in [62] the electron phase appears via exp[-iS$_1$] whereas in the standard definition via exp[iS_c] [84].

The electron return condition is: $\vec{r}(t_f)=\vec{r}(t_0)$ which leads to $I_1=\tau\sin(\omega t_0)$. Thus after performing the integration in (52) we get (using A(t) = –(cE$_0$/ω)sin(ωt) and equation (55)):

$$S_c(t_f,t_0)=-S_1(t_f,t_0)=-2U_p[I_2-I_1^2/\tau], \tag{57}$$

where $\tau=t_f-t_0, U_p=\frac{(qE_0)^2}{4\omega^2}$ is the ponderomotive energy and

$$I_1=\int_{t_0}^{t_f}dt\sin(\omega t)=\frac{\cos(\omega t_0)-\cos(\omega t_f)}{\omega}, \tag{58a}$$

$$I_2=\int_{t_0}^{t_f}dt\sin^2(\omega t)=\frac{1}{2}\tau+\frac{\sin(2\omega t_0)-\sin(2\omega t_f)}{4\omega}. \tag{58b}$$

Imposing again the return condition: $I_1=\tau\sin(\omega t_0)$, one gets from (53) the final expression for S_c in equation (57) or S_1

$$S_1(t_f,t_0)=U_p[\tau\cos(2\omega t_0)+\frac{\sin(2\omega t_0)-\sin(2\omega t_f)}{2\omega}]=2U_p\left(I_2-\frac{I_1^2}{\tau}\right). \tag{59}$$

Equation (59) agrees with equation (4) in [85].

The electron wavefunction during its classical motion staring at $t = t_0$ and ending at $t = t_f$ acquires the phase according to the formula $\exp(iS_c(t_f,t_0)=\exp(-iS_1(t_f,t_0))$. Like in the Michelson interferometer [6], the tunneling process acts as a beam splitter by splitting the electron wavefunction into two parts, a bound part which acquires the phase $-E_g\tau=I_p\tau=I_p(t_f-t_0)$ and its continuum part acquires the phase $S_c(t_f,t_0)=-S_1(t_f,t_0)$. These two parts recombine when the electron returns to the core. Thus the resulting harmonic phase upon recombination is equal to the difference of these two phases:

$$\Phi_H = S_c - I_p\tau + N\omega t_f = -S_1 - I_p\tau + N\omega t_f \tag{60}$$

for harmonic order N of energy (in a.u.)

$$N\omega = E_f + I_p = \dot{\vec{r}}^2(t_f)/2 + I_p = 2U_p[\sin(\omega t_0) - \sin(\omega t_0)]^2 + I_p\,. \tag{61}$$

We note that a similar equation to equation (61) was used earlier to predict classically maximum $3U_p$ energies in microwave ATI energies [43]. Equation (61) predicts the classical result, as reported in table 3, that maximum return energy occurs for the electron trajectory initialized at the laser phase $\omega t_0 = 0.09982\pi$. Next, such an electron accelerates in the laser electric field $E(t)$ and (assuming that its initial velocity is $v(t_0) = 0$) returns to the core at the phase $\omega t_f = 1.4003\pi = 0.7$ cycle with the kinetic energy $E_f = 3.1731U_p$.

The semiclassical 3-step recollision model proposed in [4], next derived using SFA approximation by Lewenstein *et al.* [62] and later rederived via Feynman's path-integral approach [84, 86], allows one to visualize the interaction between a strong laser field and atom or molecule. A key result of this detailed study of the 3-step model shows that dominant quantum paths follow the classical trajectories in the continuum as described in section 3. Furthermore, it was shown the existence of two apparent quantum paths (electron trajectories), Fig. 3, leading to the same final kinetic energy: a short and long path with slightly different recollision times, the short trajectories corresponding to later laser ionization time t_0 and earlier recombination time t_f than the long trajectory [87]. The accumulated harmonic phase Φ_H as predicted by equation (60) can be controlled by the phase and strength of second or third harmonic fields, i.e. $E_n(t) = E_0 \cos(n\omega t)$, $n = 2, 3$, as shown in [88-94] and also via phase matching conditions [95]. Numerical solutions of the TDSE for atoms [96] and more recently for molecules [81,97] allow for exact calculations of harmonic amplitudes and phases in HHG in atoms and MHOHG in molecules. The information gained from such TDSE simulations allows a time profile analysis of harmonics generation and a comparison with the 3-step model. Time-frequency analysis of complex signals [98] emitted as in the case of harmonics [99] proceeds via the use of wavelet transforms of the dipole acceleration, thus allowing for imaging electron trajectory recollision time with parent ions and to monitor the nuclear response in molecules to recollisions [100].

The method is based on calculating time profiles of harmonics via wavelet transforms [98,99] of the time dependent electron acceleration $a(t)$ which includes phase effects,

$$a_W(\omega,t) = \sqrt{\frac{\omega}{\pi^{1/2}\sigma}}\int_{-\infty}^{\infty}\exp(-i\omega t')\exp[-\frac{\omega^2(t'-t)^2}{2\sigma^2}]a(t')dt'\,, \tag{62}$$

σ is the width of the Gaussian time window in the transform (62) corresponding to a Gaussian frequency filter with a spectral width of ω/σ around a central frequency $\omega_0 = \omega$. The time profile analysis of a harmonic spectrum provides the recollision time t_f of an electron during the ionization process in strong fields as predicted in section 2 by classical modeling, equation (32). We illustrate in Fig. 8 such time profile of MHOHG obtained from solutions of the TDSE for the non-Born-Oppenheimer (i.e., with moving nuclei) 1-D H_2 molecules [29,100] in an electric field. Fig. 8(b) illustrates the time profile of the electron acceleration $a_{el}(t)$ and Fig. 8(c) for the proton acceleration $a_R(t)$ for particular harmonic orders $N = 57$ and 69, the latter near the cutoff. Two recollision times t_f are immediately recognized for N=57, with the short trajectory appearing near zeroes of the field at n+1/4 cycle whereas the long trajectory appears near field extrema at n and n+1/2 cycles. At the higher harmonic order N=69 near the cut-off, both short and long trajectories, merge as predicted by the classical recollision model, Fig. 3.

5. CONCLUSION

Modern ultrashort laser pulses produce electric fields whose strength approaches and also exceeds that inside atoms and molecules (table 1). This new regime of nonlinear nonperturbative radiative interactions with atoms and molecules, with its concomitant strong field ionization leads to new highly nonlinear phenomena such as high order harmonic generation, HHG, the basis of Attosecond Science [2,8]. HHG is modeled as an adiabatic, single active

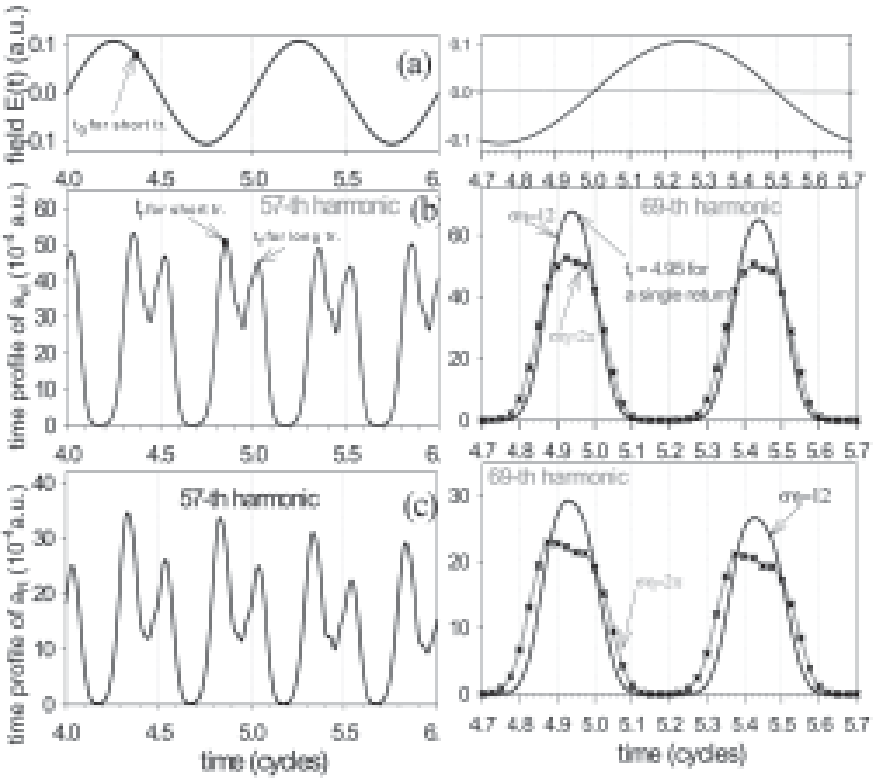

Figure 8: Left Column: (a) the Electric Field $E(t)$, (b) Time Profile of the Electron Acceleration a_{el}, and (c) Time Profile of the Proton Acceleration a_R for the Harmonic order N = 57. The Right Column Shows the Same as the Left Column but for a Higher Harmonic N = 69 (Near the Cutoff) with Different width σ for the Transforms, Equation (62)

electron, 3-step process involving: (i) under and/or above barrier ionization, the first via tunneling ionization [1-6]; (ii) electron propagation in the field thus acquiring ponderomotive energy of order $U_p = I / 4\omega^2$ (in a.u.) at recollsion time; (iii) recollision with the parent ion or collision and recombination with neighboring ions with energy of high energy coherent photons in HHG. We have summarized in section 1 simple expressions based on electrostatics and field modified Coulomb potential for the maximum electric field E_m separating the under and above barrier ionization processes [101]. In sections 2 and 3 we have derived using a simple classical model the ponderomotive energies acquired upon recollision with parent ions or collision with neighboring ions, thus defining the cutoff laws for HHG in atoms and MHOHG in molecules for linear and circular polarizations.

The main conclusion is that in the presence of intense fields, ionized electrons are completed controlled by the field, thus spawning multiple scenarios for controlling HHG by selecting electron collision and recollision paths, especially in atoms for attosecond pulse synthesis [102]. Recollision in molecules introduces more complexities, as shown for example in C_{60}, where the large polarizability of the molecule influences the recollision dynamics [103]. Similarly, recent theoretical work on nonsymmetric molecules shows the controlling influence of permanent dipole moments in MHOHG [104-106], including polarizability [107, 108] as previously shown for chemical reactions [109].

One of the main spin-offs of laser induced collision-recollision, LIERC, is Quantum Dynamic Imaging [110], earlier introduced as Laser Induced Electron Diffraction, LIED [24], tomographic imaging of molecular orbitals, TIMO [26] via molecular recollision interferometery in MHOHG [111]. Imaging molecular structure by electron diffraction using intense few-cycle laser pulses is becoming a new versatile tool for imaging molecules due to the short wavelengths (sub-nanometer) and ultrashort collision-recollision time (τ < one cycle) of the high energy photon electrons [6, 26, 112-116] produced under the conditions of ultrashort intense laser exposure. In spite of the highly nonlinear, nonperturbative response of atoms and molecules to such extreme conditions, simple classical models of laser induced collision and recollision have been the guiding models for understanding and in many cases

for controlling the physical processes that occur in this new nonperturbative regime of light-matter interaction. Extension of the simple recollision models to laser induced nuclear reactions at super-intensities ($I \geq 10^{20}$ W/cm^2) [117] have shown that such recollision models are again useful concepts [118,119] for also imaging nuclear processes [120] but will require modification due to relativistic effects and verification via appropriate Time-Dependent Dirac Equation [121].

Acknowledgements

We thank the following colleagues for "illuminating" insights in strong field physics: T. Brabec, W. Becker, P.B. Corkum, F. Krausz, M.Y. Ivanov. J.M. Rost, T. Uzer.

References

[1] T. Brabec, F. Krausz, *Rev. Mod. Phys.* **72**, 545, (2000).

[2] P. Corkum, F. Krausz, *Nature Phys.* **3**, 381, (2007).

[3] L. Keldysh, *Sov. Phys. JETP* **20**, 1307, (1965).

[4] P. B. Corkum, *Phys. Rev. Lett.* **71**, 1994, (1993).

[5] P. B. Corkum, N. H. Burnett, F. Brunel, *Phys. Rev. Lett.* **62**, 1259, (1989).

[6] P. B. Corkum, Phys. Today, **64**, 36, (2011).

[7] A. J. Verhaef *et al*., *Phys. Rev. Lett.* **104**, 163904, (2010).

[8] F. Krausz, M. Y. Ivanov, *Rev. Mod. Phys.* **81,** 163, (2009).

[9] J. I. Steinfield, "Molecules and Radiation" (MIT Press, Cambridge, USA 1985).

[10] H. Lefebvre-Brion, R.W. Field, "Spectra and Dynamics of Diatomic Molecules" (Elsevier, Holland, 2004).

[11] W. Greiner, B. Muller, J. Rafelski, Quantum Electrodynamics of Strong Fields: With an Introduction into Modern Relativistic Quantum Mechanics (Springer, Berlin, 1985).

[12] A. H. Zewail, *J. Phys. Chem. A* **104**, 5660, (2000).

[13] A. D. Bandrauk, S. Barmaki, S. Chelkowski, G.L. Kamta, in "Progress in Ultrafast Intense Laser Science", edit. K. Yamanouchi *et al*. (Springer, N. Y. 2007), Vol III, chapt. 9.

[14] S. Chelkowski, G. Yudin, A.D. Bandrauk, *J. Phys. B* **39**, S409, (2006).

[15] A. D. Bandrauk, J. Manz, M. Vrakking, *Chem. Phys.* **366**, 1, (2009).

[16] Z. Chang "Fundamentals of Attosecond Optics" (CRC Press, Taylor-Francis, USA, 2011).

[17] A. Zavriyev, P.H. Bucksbaum, in "Molecules in Laser Fields", edit. A.D. Bandrauk (Marcel Dekker Inc., NY 1994), chapt. 2.

[18] A.D. Bandrauk *et al.*, in "Molecules in Laser Fields", edit. A.D. Bandrauk (Marcel Dekker Inc., NY 1994), chapt. 4.

[19] R. S. Mulliken, *J. Chem Phys* **7**, 20 (1939).

[20] C. Cornaggia in "Progress in Ultrafast Intense Laser Science", edit. K. Yamanouchi et al, vol VI (Springer, Tokyo 2011), chapt 1.

[21] T. Zuo, A.D. Bandrauk, *Phys. Rev.* A**54**, 2511, (1995); **54**, 3254, (1996).

[22] S. Chelkowski, A. D. Bandrauk, *J. Phys. B* **28**, L723, (1995).

[23] T. Seideman, M. Y. Ivanov, P. B. Corkum, *Phys. Rev. Lett.* **75**, 2819, (1993).

[24] T. Zuo, A. D. Bandrauk, P. B. Corkum, *Chem. Phys. Lett.* **259**, 313, (1996).

[25] M. Lein, *J. Phys. B* **40**, R135, (2007).

[26] J. Itatani *et al.*, *Nature* **432**, 867, (2004).

[27] A.D. Bandrauk, H.S. Nguyen, *Int. J. Quant. Chem* **100**, 834, (2004).

[28] H. Niikura, D. Villeneuve, P. B. Corkum, *Phys. Rev. Lett.* **94**, 083003, (2005).

[29] S. Chelkowski, A. D. Bandrauk, *Phys. Rev. Lett.* **101**, 153901, (2008).

[30] A. D. Bandrauk, S. Chelkowski, H. Yu, E. Constant, *Phys. Rev. A* **56,** 2537, (1997).

[31] P. Moreno, L. Playa, L. Roso, *Phys. Rev. A* **55**, 1593, (1997).

[32] A. D. Bandrauk, H. Yu, *Phys. Rev. A* **59**, 539, (1999).

[33] M. Lein, J. M. Rost, *Phys. Rev. Lett.* **91**, 243901, (2003).

[34] U. Saalmann, J. M. Rost, *Phys. Rev. Lett.* **100**, 133006, (2008).

[35] M. Shapiro, P. Brumer "Principles of Quantum Control of Molecular Processes", (Wiley-Interscience, NY, 2003).

[36] A.D. Bandrauk, M. Delfour, C. LeBris, "Quantum Control Mathematical and Numerical Challenges", CRM Proceedings and Lectures (American Mathematical Society, Oxford Univ. Press, 2004), Vol. 33.

[37] H. Nikura *et al.*, Nature **417**, 917, (2002).

[38] K. J. Yuan, A. D. Bandrauk, *Phys. Rev. A* **81**, 063412, (2010).

[39] F. Mauger, C. Chandre, T. Uzer, *Phys. Rev. Lett.* **104**, 043005 (2010); **105**, 083002 (2010).

[40] N. B. Delone, V. P. Krainov, "Multiphoton Processes in Atoms" (Springer-Verlab, Berlin, 1994).

[41] M. J. DeWitt, R.J. Levis, *J. Chem Phys.* **108**, 1, (1998).

[42] A. D. Bandrauk, H. Z. Lu, in "Handbook of Numerical Analysis – Computational Chemistry", edit. P.G. Ciarlet, C. Le Bris (Elsevier Amsterdam, 2003) p. 803.

[43] T. F. Gallagher, Phys. *Rev. Lett.* **61**, 2304, (1988).

[44] G. Mourou, T. Tajima, *Science* **331**, 41, (2011).

[45] U. W. Rathe, C. H. Keittel, M. Protopapas, P. L. Knight, *J. Phys. B* **30**, L531, (1997).

[46] S. Selsto, E. Lindroth, J. Bengtson, *Phys. Rev.* **A79**, 043418, (2009).

[47] A. Maquet, R. Grobe, *J. Mod. Opt.* **49**, 2001, (2002).

[48] K. Codling, L. J. Frasinski, P. A. Hatherly, *J. Phys. B***22**, L321, (1989).

[49] V. H. Posthumus *et al*; J. Phys. B **28**, L 349, (1995).

[50] H. Schröder, C. J. Uiterwaal, K. L. Kompa, *Laser Phys.* **10**, 749, (2000).

[51] G. L. Kamta, A. D. Bandrauk, *Phys. Rev. A* **75**, 041401, (2007).

[52] M. Schmidt, D. Normand, C. Cornaggia, *Phys. Rev. A* **50**, 5037 (1994); *ibid*, 53, 1958 (1996).

[53] G. N. Gibson, M. Li, C. Guo, J. Neira, *Phys. Rev. Lett.* **79**, 2022, (1994).

[54] I. Ben-Itzhak *et al*., *Phys. Rev. A* **78**, 063419, (2008).

[55] G. L. Kamta, A. D. Bandrauk, *Phys. Rev. Lett.* **94**, 203003 (2005); *Phys. Rev. A* **76**, 053409 (2007).

[56] X. B. Bian, A. D. Bandrauk, *Phys. Rev. Lett.* **105**, 093903, (2010).

[57] H. R. Reiss, *Phys. Rev.A* **22**, 1786, (1980).

[58] F. Brunel, *Phys. Rev. Lett* **59**, 52, (1987).

[59] J. L. Krause, K. J. Schaffer, K. C. Kulander, *Phys. Rev. Lett.* **68**, 3535, (1992).

[60] K. J. Schafer *et al.*, *Phys. Rev. Lett.* **70**, 1599, (1993).

[61] A. L'Huillier, P. Balcou, *Phys. Rev. Lett.* **70**, 774, (1993).

[62] M. Lewenstein *et al.*, *Phys. Rev. A* **49**, 2117, (1993).

[63] A. D. Bandrauk, S. Barmaki, G. L. Kamta, *Phys. Rev. Let.t* **98**, 013001, (2007).

[64] A. D. Bandrauk, S. Chelkowski, S. Goudreau, *J. Mod. Opt.* **52**, 411, (2005).

[65] Y. Xiang, Y. Niu, S. Gong, *Phys. Rev. A* **79**, 053419, (2009).

[66] W. Becker, S. Long, J. K. McIver, *Phys. Rev. A* **50**, 1540, (1994).

[67] A. D. Bandrauk, H. S. Nguyen, *Phys. Rev. A* **66**, 031401, (2002).

[68] K. Ishikawa, *Phys. Rev. Lett.* **91**, 043002, (2003).

[69]. A. D. Bandrauk, S. Chelkowski, N. H. Shon, *Phys. Rev. Lett.* **89**, 283903, (2002).

[70] R. Kopold, W. Becker, M. Kleber, *Phys. Rev. A* **58**, 4022, (1998).

[71] T. Pfeifer *et al.*, *Phys. Rev. A* **70**, 013805, (2004).

[72] P. Lan *et al.*, *Phys. Rev. A* **74**, 06344, (2006).

[73] M. Forre, E. Mevel, E. Constant, *Phys. Rev. A* **83**, 021402, (2011).

[74] D. B. Milosevic, W. Becker, R. Kopold, *Phys. Rev. A* **61**, 063403, (2000).

[75] X. Zhou *et al.*, *Phys. Rev. Lett.* **102**, 073902, (2009).

[76] A. D. Bandrauk, H. Z. Lu, *Phys. Rev. A* **68**, 043408, (2003); **73**, 013412, (2006).

[77] M. Lein *et al.*, *Phys. Rev. Lett.* **88**, 183903, (2002).

[78] X. Xie *et al*., *Phys. Rev. Lett.* **101**, 033901, (2008).

[79] M. Kitzler *et al. Phys. Rev. Lett.* **88**, 173904, (2002).

[80] M. Lewenstein, P. Salières, A. L'Huillier, *Phys. Rev. A* **52**, 4747, (1995).

[81] G. L. Kamta, A. D. Bandrauk, *Phys. Rev. A* **71**, 053407, (2005).

[82] D. B. Milosevic, *J. Opt. Soc. Am. B* **23**, 308, (2006).

[83] D. B. Milosevic, A. F. Starace, *Phys. Rev. A* **60**, 3160, (1999).

[84] W. Becker, A. Lohr, M. Kleber, *Quant. Semiclass. Opt.* **7**, 413, (1995).

[85] C. Faria, M. Dörr, W. Sandner, *Phys. Rev. A* **55**, 3961, (1997).

[86] P. Salières *et al.*, Science **292**, 902, (2001).

[87] S. Kazamias, P. Balcou, *Phys. Rev. A* **69**, 063416, (2004).

[88] G. Sansone *et al, Phys. Rev. A* **73**, 053408, (2006).

[89] M. Y. Ivanov, *et al*., *Phys. Rev. Lett.* **74**, 2933, (1995); *Phys. Rev. A* **51** 3991, (1995).

[90] P. Antoine, A. L'Huillier, M. Lewenstein, *Phys. Rev. Lett.* **77**, 1234, (1996).

[91] G. G. Paulus, W. Becker, H. Walther, *Phys. Rev. A* **52**, 4043, (1995).

[92] C. M. Kim, C. H. Nam, *J. Phys. B* **39**, 3199, (2006).

[93] H. Merdji, *et al, Phys. Rev. A* **74**, 043804, (2006).

[94] L. Brugnera *et al, Opt. Lett.* **35**, 3994, (2010).

[95] L. E. Chipperfield *et al, Opt. Commun.* **264**, 494, (2006).

[96] K. J. Schaffer, K. C. Kulander, *Phys. Rev. Lett.* **78**, 638, (1997).

[97] K. J. Yuan, A. D. Bandrauk, *Phys. Rev. A* **80**, 053404, (2009).

[98] C. Chandre, S. Wiggins, T. Uzer, *Physica D* **181**, 171, (2003).

[99] P. Antoine, B. Piraux, A. Maquet, *Phys. Rev. A* **51**, R1750, (1995).

[100] A. D. Bandrauk, S. Chelkowski, H. Z. Lu, in "Quantum Dynamics Imaging", edit. A.D. Bandrauk and M.Y. Ivanov, (Springer, NY 2011), chapt. 2

[101] A. Scrinzi, M. Geissler, T. Brabec, *Phys. Rev. Lett.* **83**, 706, (1999).

[102] C. Ruiz *et al*, *New J. Phys.* **11**, 113045, (2009).

[103] V. R. Bhardwaj, P. B. Corkum, D. M. Rayner, *Phys. Rev. Lett.* **93**, 043001, (2004).

[104] G. L. Kamta, A. D. Bandrauk, *J. Phys. B* **38**, L339, (2005).

[105] X. B. Bian, A. D. Bandrauk, *Phys. Rev. A* **83**, 023414, (2011).

[106] D. Dimitrovski, C. P. J. Martiny, L. B. Madsen, *Phys. Rev. A* **82**, 053404, (2010).

[107] A. N. Markevitch *et al*., *Phys. Rev. A* **69**, 013401, (2004).

[108] T. Brabec, M. Coté, P. Boulanger, L. Ramunno, *Phys. Rev. Lett.* **95**, 073001, (2005).

[109] A. D. Bandrauk, E. W. S. Sedik, C. F. Matta, *J. Chem. Phys.* **121**, 7764, (2004).

[110] A.D. Bandrauk, M.Y. Ivanov, "Quantum Dynamics Imaging", edit. (Springer, NY 2011).

[111] X. Zhou *et al, Phys. Rev. Lett.* **100**, 073902, (2008).

[112] S. X. Hu, L. A. Collins, *Phys. Rev. Lett.* **94**, 073004, (2005).

[113] G. L. Kamta, A. D. Bandrauk, *Phys. Rev. A* **74,** 033415, (2006).

[114] M. F. Ciappina, C. C. Chirila, M. Lein, *Phys. Rev. A* **75**, 043405, (2007).

[115] M. Okunishi *et al., J. Phys. B* **41**, 201004 (2008); *Phys. Rev. Lett.* **106**, 063001 (2011).

[116] Y. Huismans *et al*, *Science* **331**, 61, (2011).

[117] G. Mourou, T. Tajima, *Science* **331**, 41, (2011).

[118] S. Chelkowski, A.D. Bandrauk, *Phys. Rev. Lett.* **93** 083602 (2004); *Laser Phys.* **14** 473, (2004).

[119] A. D. Bandrauk, G. K. Paramonov, AIP Conf. Proc. **1209,** 7, (2010).

[120] N. Milosevic, P. B. Corkum, T. Brabec, *Phys. Rev. Lett.* **92**, 013002, (2004).

[121] N. Milosevic, V. P. Krainov, T. Brabec, *Phys. Rev. Lett.* **89**, 193001, (2002).